Cement and Concrete Research 41 (2011) 197–208

Contents lists available at ScienceDirect

Cement and Concrete Research

journal homepage: http://ees.elsevier.com/CEMCON/default.asp

Evolution of strength, microstructure and mineralogical composition of a CKD–GGBFS binder

Piyush Chaunsali, Sulapha Peethamparan *

Department of Civil and Environmental Engineering, Clarkson University, Potsdam, NY 13699, USA

ARTICLE INFO

Article history:
Received 6 July 2010
Accepted 17 November 2010

Keywords:
Cement kiln dust (CKD) (D)
Ground granulated blast furnace slag (GGBFS) (D)
Characterization (B)
X-ray diffraction (B)
Thermogravimetry (B)
Scanning electron microscopy (B)

ABSTRACT

Characterization of a nontraditional binding material containing cement kiln dust (CKD) and ground granulated blast furnace slag (GGBFS) is discussed in this paper. Significant compressive strength was obtained for a CKD–GGBFS blend with 70% CKD and 30% GGBFS at a water-to-binder ratio of 0.40 after 2 days of curing at elevated temperature. Similar strength was also obtained for the samples subjected to normal moisture curing over a period of 28 days. The compressive strength increased with additional moist curing in both the cases. The microstructural and the mineralogical examinations show that the strength development was mainly due to the formation of calcium silicate hydrate (C-S-H). In addition to normal C-S-H, aluminum and magnesium incorporated C-S-H phases were also present in the CKD–GGBFS blends. The formation of ettringite appears to be a contributing factor in early age strength development of CKD–GGBFS binder.

Published by Elsevier Ltd.

1. Introduction

The adverse effect of cement production on the environment can be significantly reduced by using high volume replacement of cement with supplementary cementing materials or finding more eco-friendly concrete. The development of sustainable and eco-friendly concrete requires novel alternative binding materials with minimum cement content. The development of cement-free binders by activating industrial by-products containing aluminosilicates such as, blast furnace slag (GGBFS) and fly ash, using strong alkaline solutions has received wide attention from researchers in recent years [1–8].

Ground granulated blast furnace slag (GGBFS) has been used as a supplementary cementitious material in Portland cement concrete because of its favorable latent hydraulic properties. Interestingly, the reaction of GGBFS when directly exposed to water is a very slow process. It has been reported that the low reactivity of the GGBFS is due to the formation of a protective layer around a slag grain which inhibits further reaction [9]. Dissolution can only be reinitiated if, somehow, this reaction layer is removed or converted to a permeable layer, and the unreacted surface again comes into contact with water. When used as a supplementary cementitious material in concrete, the high alkaline environment resulting from cement hydration dissolves the glassy structure of the coating, thereby exposing the anhydrous surface for further hydration. Thus, the use of GGBFS as a sole binder in concrete potentially requires an external supply of activator that can attack the glassy structure and increase the reactivity of GGBFS.

Several methods for accelerating the reactivity of slag, including thermal and chemical activations, have been investigated in the past [10,11]. Based on these studies, the major factors that influence the strength development in activated binder are thermal curing conditions, type and concentration of the activator, and specific surface area of the slag [12]. Dissolution of slag and formation of initial reaction products in alkali-activated slag depend on the initial pH of the activating solution. However, later stage hydration is dominated by the reaction of anions released from the activator and calcium ions released from slag rather than the initial pH of the activator solution [13]. Activation of aluminosilicate materials with alkalis generally requires heat curing for the formation of alkali-aluminosilicates, especially when the activating solution does not contain sufficient amount of soluble silica. A wide array of temperatures ranging from 20 °C to 100 °C has been used for enhancing the reaction kinetics and the strength development of alkali-activated binders [14–16]. Calcium sulfate, another constituent of the CKD, has also been found to activate the slag resulting in the precipitation of ettringite [17,18].

In addition to studies on using commercially available alkalis for GGBFS activation, preliminary results on using industrial by-products such as cement kiln dusts (CKDs) as activators for GGBFS have also been reported [19–21]. Cement kiln dust, a fine powdery waste material carried by hot cement kiln gases, and collected through electrostatic precipitators, is generated in large quantities by the cement industry. Many of the CKDs contain significant amounts of alkalis, sulfates and free calcium oxide [21–24]. The chemical composition of cement kiln dust makes it a potential material for activating GGBFS [21].

* Corresponding author. Tel.: +1 315 268 4435; fax: +1 315 268 7985.
E-mail address: speetham@clarkson.edu (S. Peethamparan).

0008-8846/$ – see front matter. Published by Elsevier Ltd.
doi:10.1016/j.cemconres.2010.11.010

In this article, the potential of a CKD (with low free lime, high alkali and sulfate contents) in accelerating the reaction kinetics of a grade 100 GGBFS is investigated. In most of the existing applications for the beneficial utilization of CKDs, such as soil stabilization, better performance is obtained with CKDs containing higher free lime, since underlying strength development mechanisms for these applications involve significant free lime consumption [23]. The motivation for selecting low free lime content CKD in the present study that had high alkali and sulfate contents is based on our hypothesis that the activation of GGBFS by the alkalis and sulfates present in the CKD plays a dominant role in the strength development in the CKD–GGBFS system. This, if proven, will open a new avenue for the beneficial utilization of low free lime content CKDs which otherwise need to be land filled. The GGBFS was blended with cement kiln dust under different conditions, and both the fresh and hardened properties of the resulting binder were studied. A detailed mineralogical and morphological characterizations were also carried out to identify the reaction products of the CKD–GGBFS binder. The mineralogical composition and the microstructural properties of the developed cement-free binder were investigated mainly using X-ray diffraction (XRD), thermogravimetric analysis (TGA) and scanning electron microscopy (SEM) coupled with energy dispersive X-ray (EDX) techniques. The scope of the research was limited in finding the optimum proportion of the CKD and GGBFS, the optimum temperature for curing and the characterization of the resulting hardened CKD-GGBFS paste with respect to the microstructural and mineralogical compositions.

2. Experimental program

2.1. Materials

In this study, a grade 100, ASTM C 989 compliant, GGBFS and a low free lime content CKD were used for developing the cement-free binder. The chemical compositions of these materials are given in Table 1. The total calcium oxide (CaO) content of the CKD was 61.15%, which includes ~5% of free lime along with the combined CaO present in calcite ($CaCO_3$) and anhydrite ($CaSO_4$). A separate loss on ignition (LOI) analysis yielded a value of 23.40% for the CKD indicating that the predominant calcium containing phase in the CKD is calcite. The dominance of calcite presence in the CKD can also be clearly evident from the XRD and thermal analysis of the CKD powder presented in Fig. 1 (A) and (B) respectively. In addition to calcite, the oxide composition of the CKD used in the present study contained significant amounts of alkalis (Na_2O and K_2O) and sulfates. The GGBFS used for the study had a Si/Al ratio of approximately 3.42.

Fig. 1 (A) shows the XRD pattern of slag with a halo in between 25° and 35° (2θ°) range showing the amorphous nature of the material. Fig. 1 (A) also shows the XRD pattern of the CKD, which confirmed the presence of calcite, quick lime, anhydrite and arcanite minerals but did not show any indication for the presence of the amorphous phases. The average particle sizes of the GGBFS and CKD were ~7 μm and ~4 μm respectively (Fig. 1 (C)). The particle size distributions were determined by a laser particle size analyzer using isopropyl alcohol as the dispersing agent.

Table 1
Chemical composition of materials.

Chemical composition	Percent weight	
	GGBFS	CKD
SiO_2	36.00	14.55
Al_2O_3	10.53	4.46
Fe_2O_3	0.67	2.11
CaO	39.80	61.15
MgO	7.93	3.84
Na_2O	0.27	0.80
K_2O	0.15	3.45
SO_2	2.11	10.62
Total	97.46	100.98
Additional information		
Na_2O_{eq}	0.32	3.10
Loss on ignition	3.00	23.40

Note: the minor components such as TiO_2, MnO and P_2O_5 present in slag are excluded from the oxide composition.

2.2. Sample preparation

2.2.1. Determination of optimum temperature for heat curing

The present study is based on the hypothesis that the alkalis, free lime and sulfates present in the CKD can accelerate the reactivity of GGBFS in a very similar way as the commercial alkalis activate slag. Hence, as we have seen in alkali activation of GGBFS [14–16], temperature may also play a significant role in strength development of CKD–GGBFS binder. To find the optimum temperature of curing to get the maximum compressive strength, 50 mm × 50 mm × 50 mm size paste specimens were prepared, heat cured at various temperatures, and then tested for the compressive strength. A binder proportion of 50% CKD and 50% GGBFS with a water-to-binder ratio of 0.40 was used for determining the optimum temperature. The GGBFS and CKD were homogenized in the dry condition prior to the addition of the water, and the paste samples were prepared using this dry homogenized mixture as per ASTM C 305 procedure. The specimens were demolded after 24 h, wrapped in aluminum foils and subsequently heated at 50, 60, 75, 90 and 100 °C for a period of 48 h in a laboratory oven. The specimens were then removed from the oven, allowed to cool down to room temperature and the compressive strengths were determined as per ASTM C 109. Fig. 2 shows the effect of curing temperature on the compressive strength development of CKD–GGBFS binder. The maximum compressive strength was obtained for the specimens subjected to 75 °C heat curing.

2.2.2. Determination of optimum binder proportion

To determine the optimum binder proportion for achieving the maximum compressive strength, samples containing 40, 50, 60, 70, 80 and 100% (by mass) CKD were prepared and tested. The specimens were prepared following the same procedures described in the previous section (Section 2.2.1). Fig. 3 shows the compressive strength of CKD–GGBFS binder with varying CKD contents after 48 h of heat curing at 75 °C. The maximum strength of ~25 MPa was obtained for a binder combination of 70% CKD and 30% GGBFS. Hence, this optimum binder proportion was used for the rest of the study.

2.2.3. Workability, setting time and compressive strength

The workability (flow value) and the setting time of the developed binder were evaluated as per ASTM C 1437 [25] and ASTM C 191 [26], respectively. In the standard test method, the paste used for determining the setting time should be prepared using the normal consistency water content. In the present study, setting time test was performed on a paste prepared at specific water-to-binder ratio (w/b) rather than using the normal consistency water content. The purpose of the test was to evaluate the setting time of the CKD–GGBFS binder with a specific w/b ratio. The specimens to be tested for compressive strength were demolded after 24 h of casting, wrapped in aluminum foils and subjected to heat curing in an oven for 48 h at the optimum temperature (75 °C). After the heat curing samples were allowed to cool down to ambient temperatures, one set of these samples was tested for the compressive strength and another set of samples was subjected to soaking in saturated lime water to explore the potential for further strength gain due to additional moist curing. A third set of

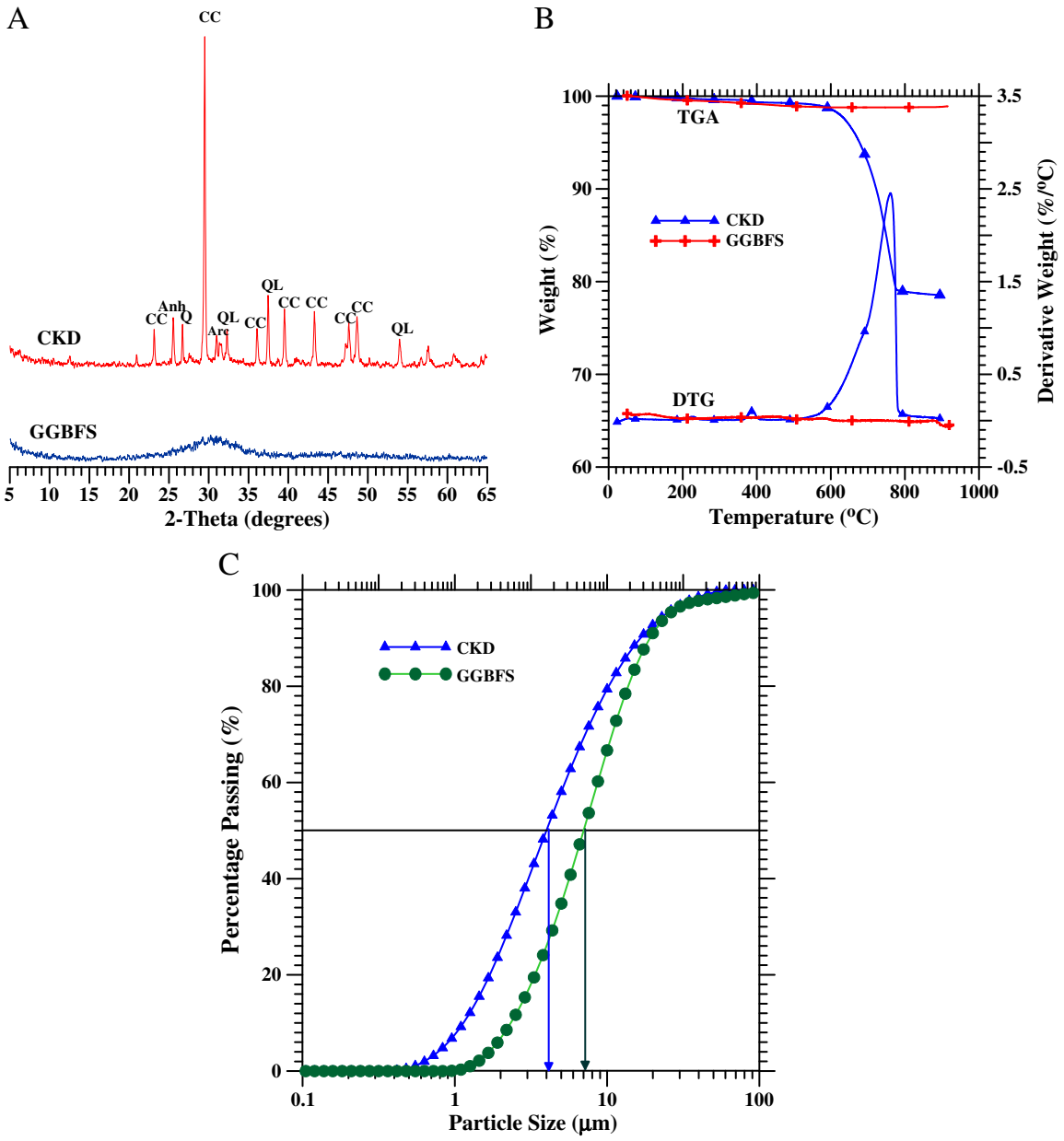

Fig. 1. Physical and mineralogical compositions of CKD and GGBFS: (A) X-ray diffraction patterns (CC—calcite, Anh—anhydrite, QL—quick lime, Arc—arcanite, Q—quartz) (B) TGA/DTG curves, and (C) particle size distribution.

samples was soaked in the saturated lime water immediately after demolding the specimens without being subjected to heat curing. The compressive strengths were determined as per ASTM C 109 for all the cases. For comparison purposes, workability, setting time, and compressive strengths of neat CKD paste were also evaluated.

2.2.4. Mineralogical and morphological characterization

Small cylindrical companion specimens were also prepared in cylindrical polypropylene vials for microstructural analysis of CKD–GGBFS (optimum proportion) binders and neat CKD paste. The cylindrical samples were cut into small cubic specimens after four different curing conditions; (1) 24 h in ambient temperature (designated by "24 h(A)"), (2) 48 h of heat curing in the oven at 75 °C (designated by "24 h(A) + 48 h (H)"), (3) 28 days in saturated lime water followed by 48 h heat curing (designated by "24 h(A) + 48 h (H) + 28 (L)"), and (4) 28 days of wet curing in saturated lime water without initial heat curing (designated as "24 h(A) + 28 (L)"). The small specimens were soaked in acetone to quench further hydration [27]. Samples soaked in acetone were dried in vacuum desiccators for 1 day at room temperature prior to the examination. A part of the vacuum dried cubic specimens was used for the SEM examination. The rest of the samples were ground until it passed through 75 micrometer (μm) size sieve. The sieved powder material was used for the TGA and the XRD analyses.

2.3. Test methods

2.3.1. Thermogravimetric analysis (TGA/DTG)

Thermogravimetric analysis was performed using a Perkin-Elmer thermogravimetric analyzer. In this test, a powdered sample (passing through 75 μm sieve) weighing 25 ± 2 mg was heated in a nitrogen environment from 50 °C to 1000 °C at the rate of 10 °C per minute. The nitrogen gas flow rate was kept at 40 ml/min. The weight loss curves

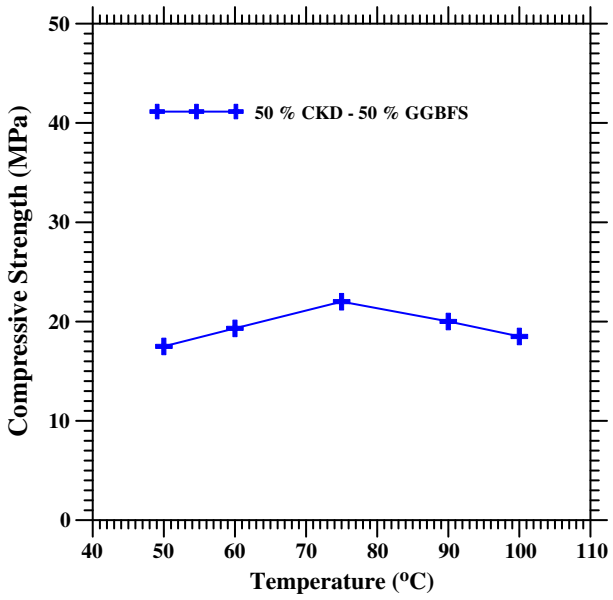

Fig. 2. Effect of curing temperature on the compressive strength of CKD–GGBFS binder after 48 h of heat curing (w/b—0.40).

(TGA) and differential weight loss curves (DTG) acquired were used for identifying the phases present in the system.

2.3.2. X-ray diffraction analysis (XRD)

X-ray diffraction measurements were carried out using the Bruker DX-8 diffractometer. CuKα radiation with a wavelength of 1.5405 Å was used. Samples were scanned between 5° and 65° (2θ) in continuous mode with an integrated step scan of 0.02° per second. Randomly oriented powder (prepared as per Section 2.2.4) samples were used for the XRD analysis.

2.3.3. Scanning electron microscopy (SEM)

Scanning electron microscopy (SEM) was used to examine the fractured specimen surfaces in the secondary electron imaging mode using a JEOL JSM-7400F electron microscope. Cube-shaped specimens prepared as described earlier were fractured to expose clean fresh surfaces. The specimens were then mounted on aluminum stubs using carbon paint, and the exposed fractured surfaces were sputter-coated with gold. The lower electron image (LEI) detector was used for taking images. Energy dispersive X-ray (EDX) patterns were obtained at selected locations using an Oxford Instruments INCA System.

3. Results and discussions

3.1. Setting time and flow test

Fig. 4 (A) shows the setting time of neat CKD, GGBFS and CKD–GGBFS pastes. The initial setting times were determined to be 90 and 240 min for the neat CKD and the CKD–GGBFS pastes, respectively. The neat GGBFS paste did not set even after 24 h.

In neat CKD paste, the initial exothermic reaction (conversion of the free lime (CaO) to $Ca(OH)_2$) consumes considerable amount of

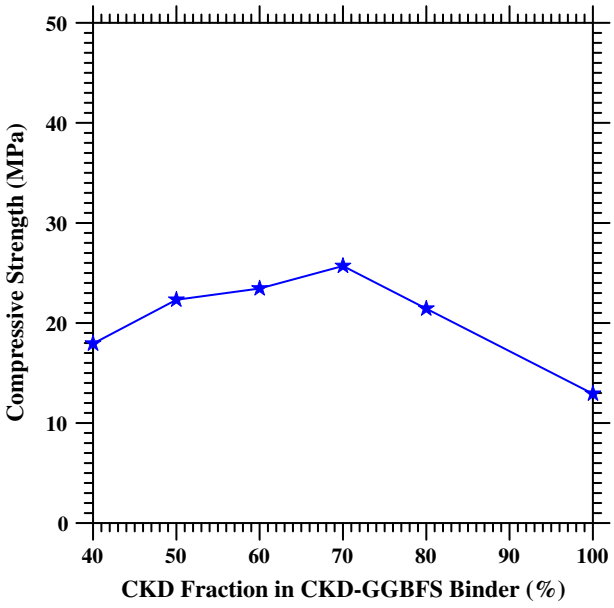

Fig. 3. Effect of CKD dosage on the compressive strength of CKD–GGBFS binder after 48 h of heat curing at 75 °C (w/b—0.40).

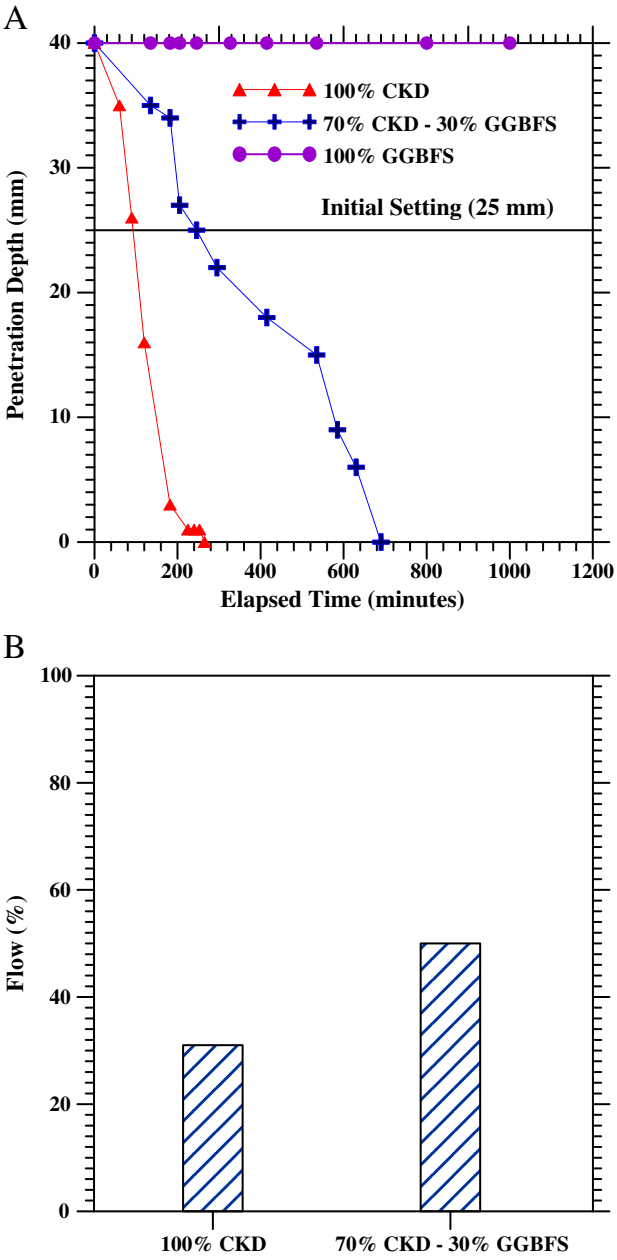

Fig. 4. Early age properties of CKD and CKD–GGBFS pastes: (A) setting time, and (B) flow value.

mixing water and results in the formation of crystalline minerals such as calcium hydroxide (CH) and ettringite (E). These minerals cause the early stiffening and setting in neat CKD paste, whereas the dilution effect caused by the addition of GGBFS in CKD–GGBFS blend results in the formation of calcium hydroxide, and ettringite, at a slower rate resulting in a delayed setting time.

Fig. 4 (B) shows the workability (flow values) of the neat CKD and CKD–GGBFS pastes. The flow value of the neat CKD paste was only 30% whereas the flow value of the CKD–GGBFS paste was ~50%.

3.2. Compressive strength

Fig. 5 shows the compressive strength of CKD–GGBFS binder after 48 h of heat curing and the effect of subsequent wet curing for an extended period of time. The compressive strength of neat CKD paste was ~12 MPa after 48 h of heat curing at 75 °C. Additional wet curing of the neat CKD pastes did not yield any improvement in its strength. A compressive strength of 25 MPa was obtained for CKD–GGBFS binder after 48 h of heat curing at 75 °C. The strength increased significantly when the heat cured specimens were subjected to further wet curing in saturated lime water up to 56 days. Only marginal improvement in compressive strength was observed beyond 56 days of wet curing. Fig. 5 also presents the strength gain of CKD–GGBFS paste cured in saturated limewater without the initial 48 h of heat curing. A compressive strength of ~30 MPa was obtained at the end of 28 days. Thus, irrespective of the curing methods, the CKD–GGBFS binder achieved an appreciable compressive strength.

3.3. Mineralogical characterization

3.3.1. Neat CKD paste

The mineralogical composition of the CKD paste was determined using the TGA/DTG (Fig. 6 (A) and (B)) and XRD analyses (Fig. 6 (C)). The reaction products identified in 24 hour old unheated CKD paste were ettringite (~80 °C), gypsum (~120 °C), and calcium hydroxide (~400 °C). A major weight loss was also observed at 700 °C due to the decomposition of the calcite that was present originally in the CKD powder (Fig. 6 (B)). The formation of gypsum and calcium hydroxide can be attributed to the anhydrite and quick lime present in the CKD powder (Fig. 1 (A)). A significant increase in the ettringite peak intensity at the expense of gypsum was observed for the neat CKD subjected to 48 h of heat curing. Only a slight change in the calcium hydroxide peak was observed between the 24 hour old unheated and the 48 hour heat cured CKD pastes discounting the occurrence of any significant pozzolanic reaction in the neat CKD paste. The presence of calcium hydroxide in both samples, one subjected to heat curing and the other subjected to heat curing followed by saturated lime water curing, also indicates the absence of any possible pozzolanic reaction in the CKD paste, which otherwise would have consumed the calcium hydroxide (Fig. 6 (B)). The prolonged curing in the saturated lime water after 48 h of heat curing did not affect the intensity of the CH peak, though there is a moderate increase in ettringite peak intensity. The calcite that was present in the original CKD powder did not undergo any modifications. Hence as expected, the size of the calcite peak was not affected by changes in the curing conditions.

The key findings of thermal analysis (TGA/DTG) such as the presence of ettringite, calcium hydroxide, gypsum and calcite in 24 hour old unheated CKD paste, formation of additional ettringite at the expense of gypsum in 48 h heat cured specimens, and the presence of unaltered calcium hydroxide peaks in samples cured at different conditions were also validated by XRD analysis (Fig. 6 (C)).

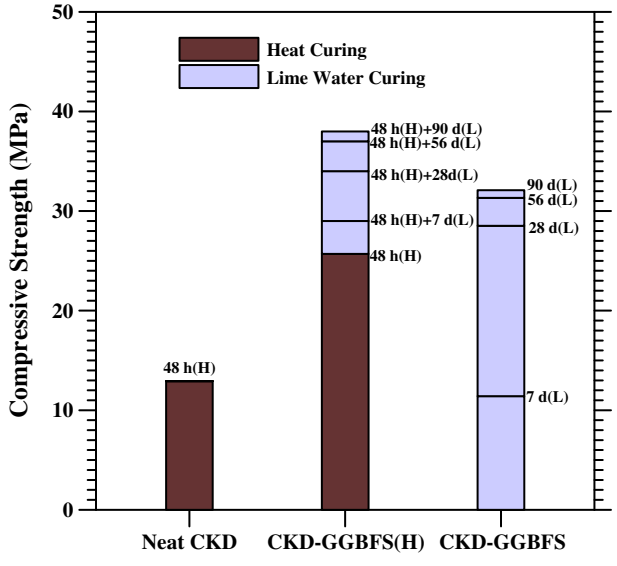

Fig. 5. Effect of curing regimes on the compressive strength of neat CKD and CKD–GGBFS pastes (w/b—0.40).

3.3.2. CKD–GGBFS binder

The TGA/DTG results of CKD–GGBFS paste exposed to different curing conditions are shown in Fig.7. Ettringite, gypsum and CH were identified in CKD–GGBFS paste after 24 h of hydration (mainly due to the reaction of CKD with water). As observed in neat CKD paste, the calcite peak, which is not a reaction product, rather a component of the original CKD powder was also present. However, compared to neat CKD paste, the size of the peaks were substantially smaller in the blended system, which was expected due to the dilution effect. In addition to the dilution effect, reduction in peak size for some phases relative to the neat CKD system is also possible if these phases are consumed for the formation of new phases (for example: formation of C-S-H at the expense of CH). For the samples heat cured at 75 °C for 48 h, the CH peak completely disappeared from the CKD–GGBFS system. Even though the slag is widely considered as hydraulic, in this study, it appears that a small portion of the glassy slag reacted with the CH to form secondary C-S-H. Another reason for the disappearance of the CH from the system could be due to the possibility of incorporation of the additional Ca^{2+} ions into the low Ca/Si ratio bearing C-S-H formed from the hydration of slag. In addition to the disappearance of CH, the TGA curves (Fig. 7 (A)) show significant but gradual weight loss between 200 and 400 °C. A gradual weight loss in this temperature range could be attributed to the dehydroxylation of C-S-H [28–30]. The slope of the TGA curve between 200 and 400 °C further increased with additional wet curing indicating additional C-S-H formation in the blended system. For the wet cured CKD–GGBFS paste without any heat curing, the TGA and DTG patterns resembled those of 48 h heat cured samples, indicating the equivalent property development in 48 h heat cured and 28 day wet cured samples.

The X-ray diffraction patterns of the CKD–GGBFS binder shown in Fig. 7 (C) also confirm the presence of CH in the 24 hour old sample [24 (A)], the disappearance of the same peaks in heat cured samples [24(A) + 48 h (H)], the increase in the intensity of the ettringite peak due to additional wet curing [24 h(A) + 48 h (H) + 28 (L)] and the increase in the intensity of the ettringite peak in wet cured samples without any heat curing [24 h(A) + 28 (L)].

3.4. Morphological studies

3.4.1. Neat CKD paste

Four representative SEM micrographs of the neat CKD paste samples that had been subjected to 48 h of heat curing at 75 °C are presented in Fig. 8. A number of mineralogically and morphologically different crystals were identified with the help of EDX analysis. Three locations from which the EDX secured are marked as 1, 2 and 3 in the

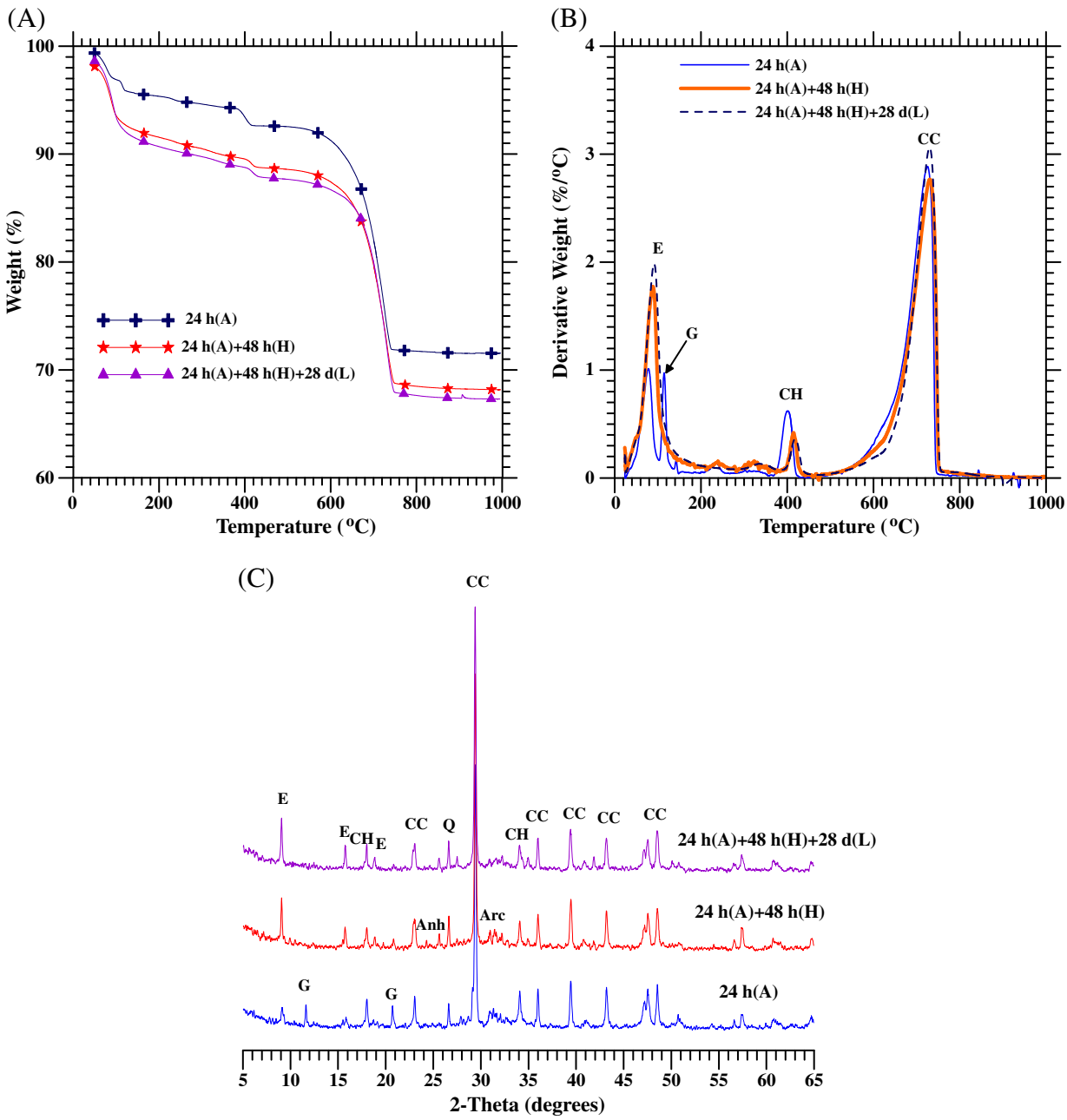

Fig. 6. Mineralogical characterization of CKD paste: (A) TGA curves, (B) DTG curves, and (C) XRD patterns (E—ettringite, CH—calcium hydroxide, CC—calcite, Anh—anhydrite, Arc—arcanite, Q—quartz, G—gypsum).

micrographs. The following phases were identified in the system based on the EDX analysis and the morphology; (i) sodium potassium sulfate (EDX at location 1), (ii) calcium carbonate crystals (EDX at location 2), (iii) ettringite (Fig. 8(C)), and (iv) C-S-H like gel with a high Ca/Si ratio (EDX at location 3). The 'Au' peak that appeared in all EDX spectrums is due to the gold sputter coating used for preparing the SEM samples. Overall, the microstructure of the 48 h heat cured (75 °C) CKD paste appeared to be porous as seen in Fig. 8 (D).

3.4.2. CKD–GGBFS binder

Representative SEM micrographs of CKD–GGBFS binder after 48 h of heat curing are presented in Fig. 9. Overall, the microstructure of these specimens had a relatively finer matrix and appeared to be less porous and more compact compared to neat CKD paste. The microstructure consisted of C-S-H like gel with variable amounts of Al and Mg incorporated phases. The presence of Mg and Al substituted C-S-H phases, as identified in the CKD–GGBFS binder in the present study, has also been reported in alkali-activated GGBFS and GGBFS–OPC blends [31–33]. The chemical composition of both CKD and the GGBFS used in the present study, as seen in Table 1, consists of significant amounts of magnesium (Mg^{2+}) and aluminum (Al^{3+}) ions containing oxides. Apart from magnesium (Mg^{2+}) and aluminum (Al^{3+}) ions, small amounts of alkali were also found to be incorporated in the C-S-H like gel structure. The Ca/Si ratio of the C-S-H phases identified in the CKD–GGBFS paste was qualitatively determined to be approximately 2 (EDXs at locations 4 and 5). Please note that the EDX spectra presented in this study were collected from a fractured specimen surface (not from the polished specimens), hence the height of the peaks were used as a qualitative measure rather than a quantitative one. In addition to C-S-H gel, fine needle-like ettringite crystals were also found in the microstructure of CKD–GGBFS paste (Fig. 9 (A) and (B)).

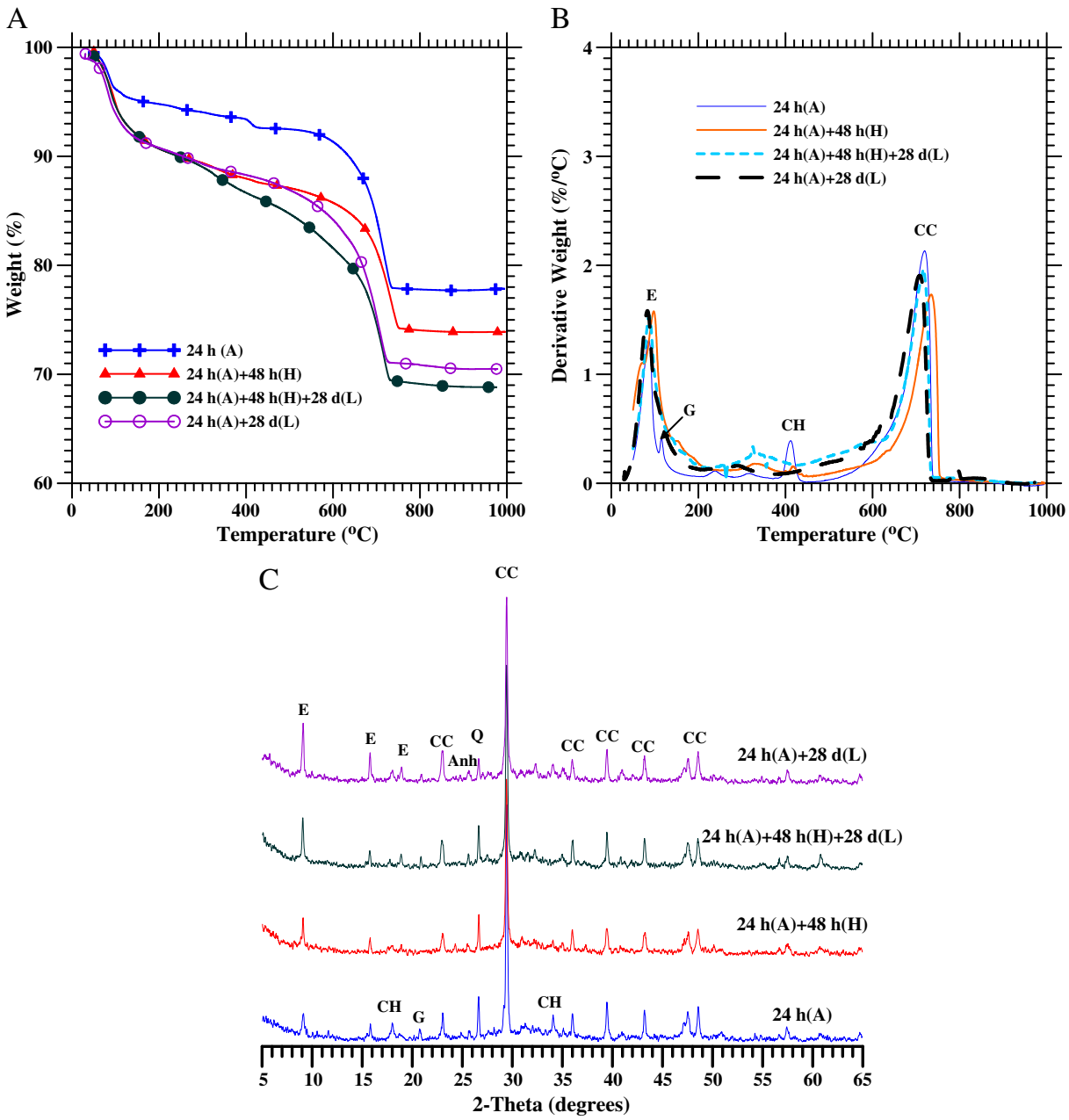

Fig. 7. Mineralogical characterization of CKD–GGBFS paste: (A) TGA curves, (B) DTG curves, and (C) XRD patterns (E—ettringite, CH—calcium hydroxide, CC—calcite, Anh—anhydrite, Q—quartz, G—gypsum).

Fig. 10 shows the effect of additional wet curing on the microstructure of the CKD–GGBFS paste after the initial heat curing. The microstructure of these samples also appeared to be dense and compact. The Ca/Si ratio of the C-S-H in these samples was observed to be varying approximately between 1 and 2 (EDX patterns at locations 6 and 7).

The microstructure of continuously wet cured CKD–GGBFS paste is shown in Fig. 11. As seen in heat cured samples (Figs. 9, 10 and 11), an extensive formation of C-S-H gel with Al and Mg substitution was found in wet cured samples as well. The morphology, as evident from the micrograph marked as "D" at high magnification in Fig. 11, appeared to be flaky, similar to the heat cured samples. It appears that the Ca/Si ratio of the C-S-H (EDX locations 8 and 9), here in this case is also approximately 2. These observations from the SEM examination show that heat cured and wet cured samples did not have any significant difference as far as the microstructural development is concerned. The presence of dense microstructure and presence of calcium–aluminate–magnesium–silicate hydrate gel (C-A-M-S-H) in both of these cases resulted in high strength. However, in the wet cured process, it requires considerable amount of time to develop the same amount of strength compared to heat cured samples.

4. Discussion

The present study demonstrated that blending of CKD and GGBFS at the optimum proportion can produce a binder with a compressive strength of ~25 MPa after heat curing the resulting paste for 48 h. The compressive strength of the specimens increased with additional wet curing in saturated lime water. It was also shown that a compressive strength of ~28 MPa could be obtained for 28 day normal wet cured specimens even without initial heat curing. With further wet curing the compressive strength increased up to ~38 MPa in the heat cured

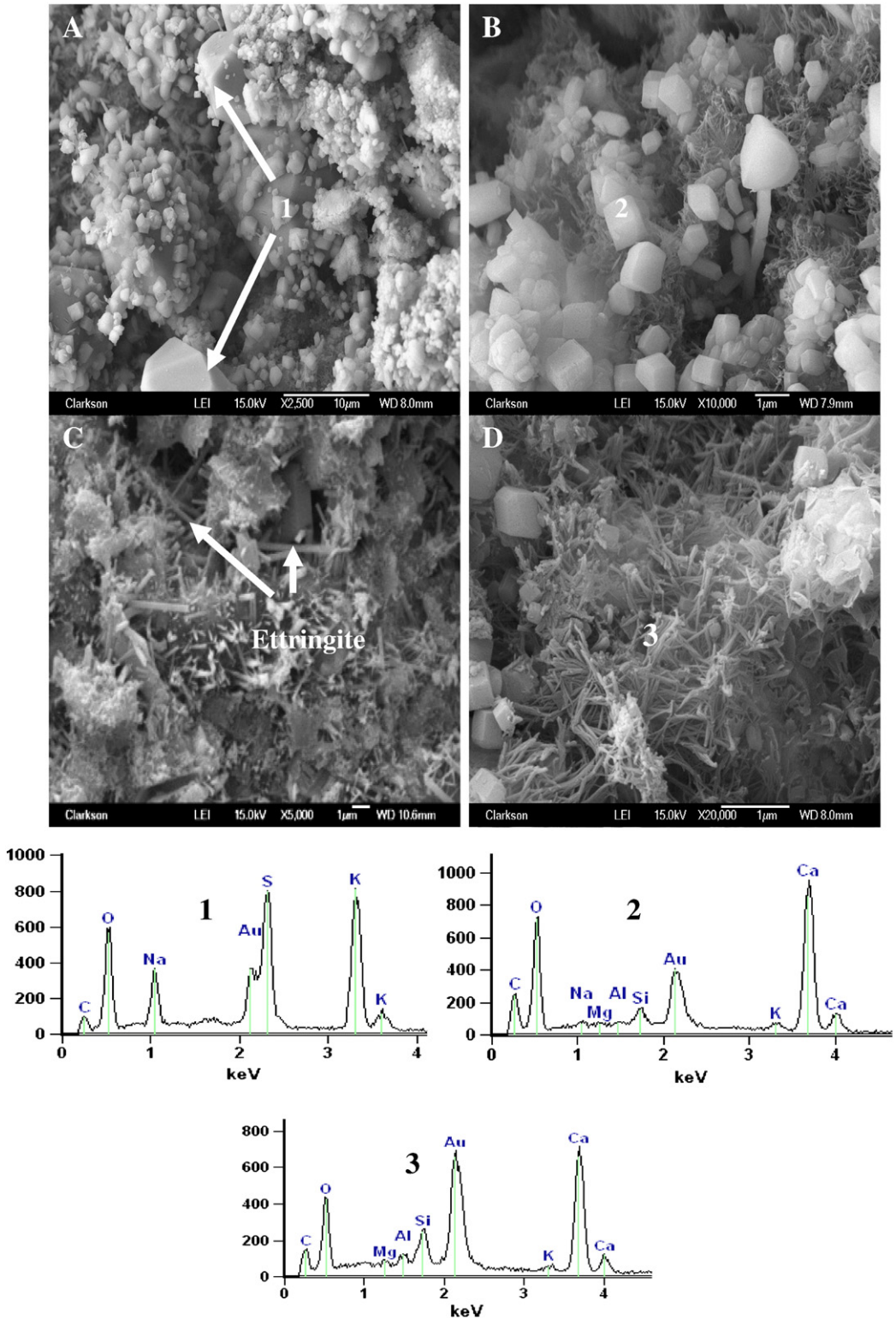

Fig. 8. SEM micrographs of 48 h heat cured neat CKD paste with EDX secured from locations 1, 2 and 3.

samples and ~32 MPa in the normal wet cured sample by the end of 90 days (Fig. 5). It should be noted that the compressive strength of the neat CKD paste was only about 12 MPa after 48 h of heat curing and the neat GGBFS paste did not even set after 24 h.

The TGA and XRD analyses identified ettringite, gypsum and calcium hydroxide phases in the CKD–GGBFS paste at an early age (24 hour old, before heat curing) and the remnant of the calcite from the CKD powder. At later ages, the CH and gypsum peaks disappeared and the height of the ettringite peak slightly increased. It is interesting to note that the formation of the ettringite was preferred in both the CKD and CKD–GGBFS samples irrespective of the curing temperatures. This could be due to the abundance of the sulfates present in these systems compared to the OPC pastes. The disappearance of the CH from the system could be due to a secondary reaction between the CH and some of the glassy slag particles or could be due to the incorporation of additional Ca^{2+} ions from the CH into the low Ca/Si

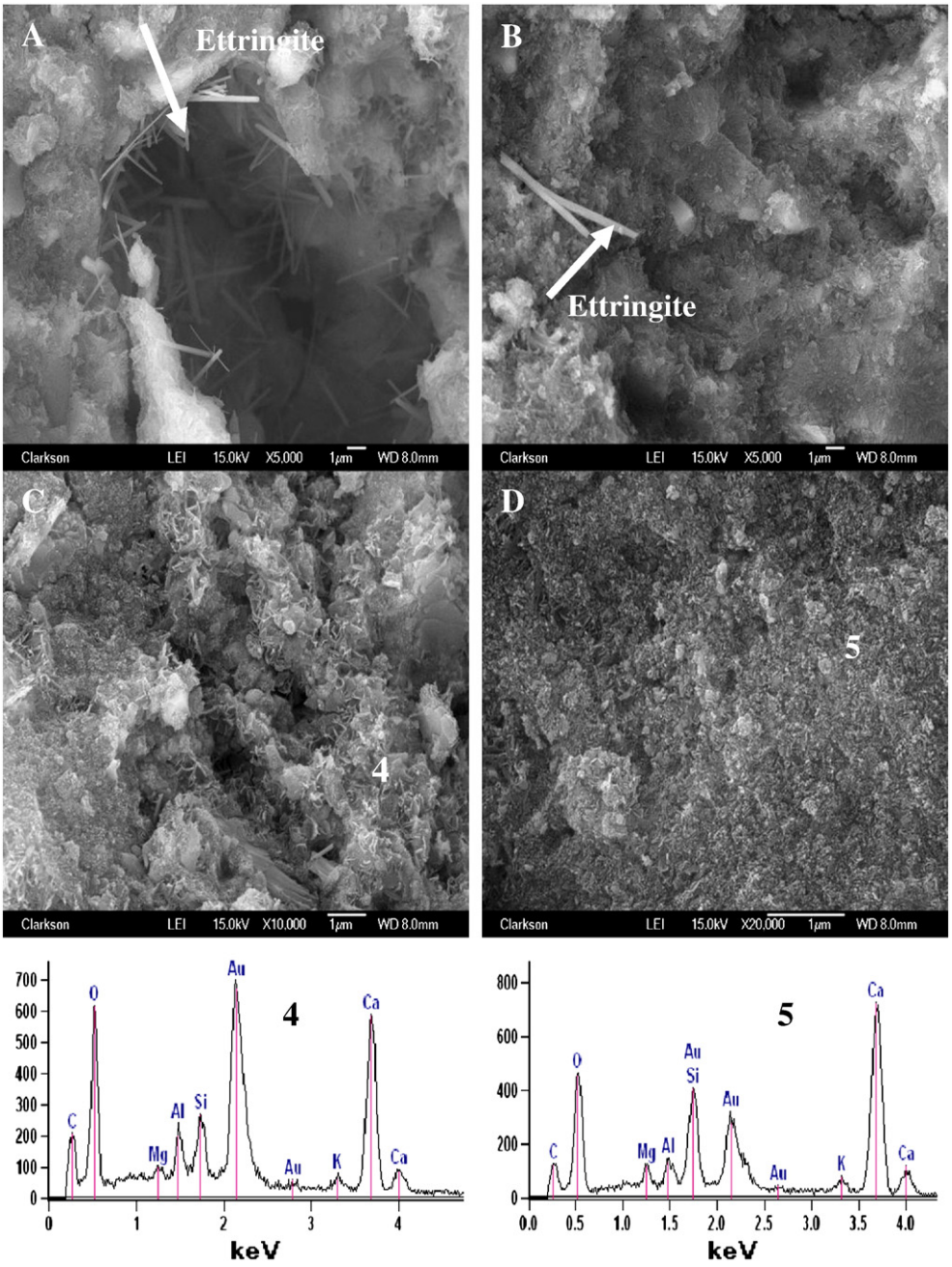

Fig. 9. SEM micrographs of CKD–GGBFS paste after 48 h of heat curing with EDX patterns at locations 4 and 5.

ratio C-S-H formed due to the hydration of slag by itself in the system. The increase in the slope of the TGA curve between 200 and 400 °C with an increase in curing period of the samples could be taken as a measure of the amount of C-S-H formed in the system [28,29]. The larger slope of the curve obtained for samples with higher compressive strength is consistent with this conclusion. As described earlier in Figs. 9–11, the SEM examination of the samples also revealed the extensive presence of C-S-H in CKD–GGBFS binder. Majority of the C-S-H phase identified was magnesium, aluminum and potassium substituted C-S-H. The Ca/Si ratio was determined to be ~2 in most of the places, and being ~1 in a few of the places. With the increase in slag loading, the Ca/Si ratio of the C-S-H gel decreases from around 1.8 for plain Portland cement paste to 1.1–1.2 in the extreme case of a paste of an alkali-activated slag containing no Portland cement [31,32]. The hydration of GGBFS results in the formation of C-S-H gel having a low Ca/Si ratio [17]. The degree of reaction of the GGBFS was expected to be higher in CKD–GGBFS systems the in presence of alkalis and sulfates mainly because of the activation effect of these components on the slag. The presence of higher Ca/Si (~2) ratio C-S-H present in the microstructure of the CKD–GGBFS system could be due to the incorporation of the additional Ca^{2+} ions from the CH into the low Ca/Si ratio C-S-H formed by the hydration of slag. The consumption of calcium hydroxide for the possible secondary pozzolanic reaction between some of the glassy slag particles and CH could also be another reason for the presence of C-S-H with higher Ca/Si ratio in the CKD-activated system. Based on the SEM and TGA analyses, the binding property and strength development in CKD–GGBFS binder can mainly be attributed to the C-S-H gel formation. Although the ettringite was found in the activated system, most of it was formed during the initial period of the activation. Only moderate changes were observed in the ettringite peaks (XRD and TGA) in the specimens subjected to extensive wet

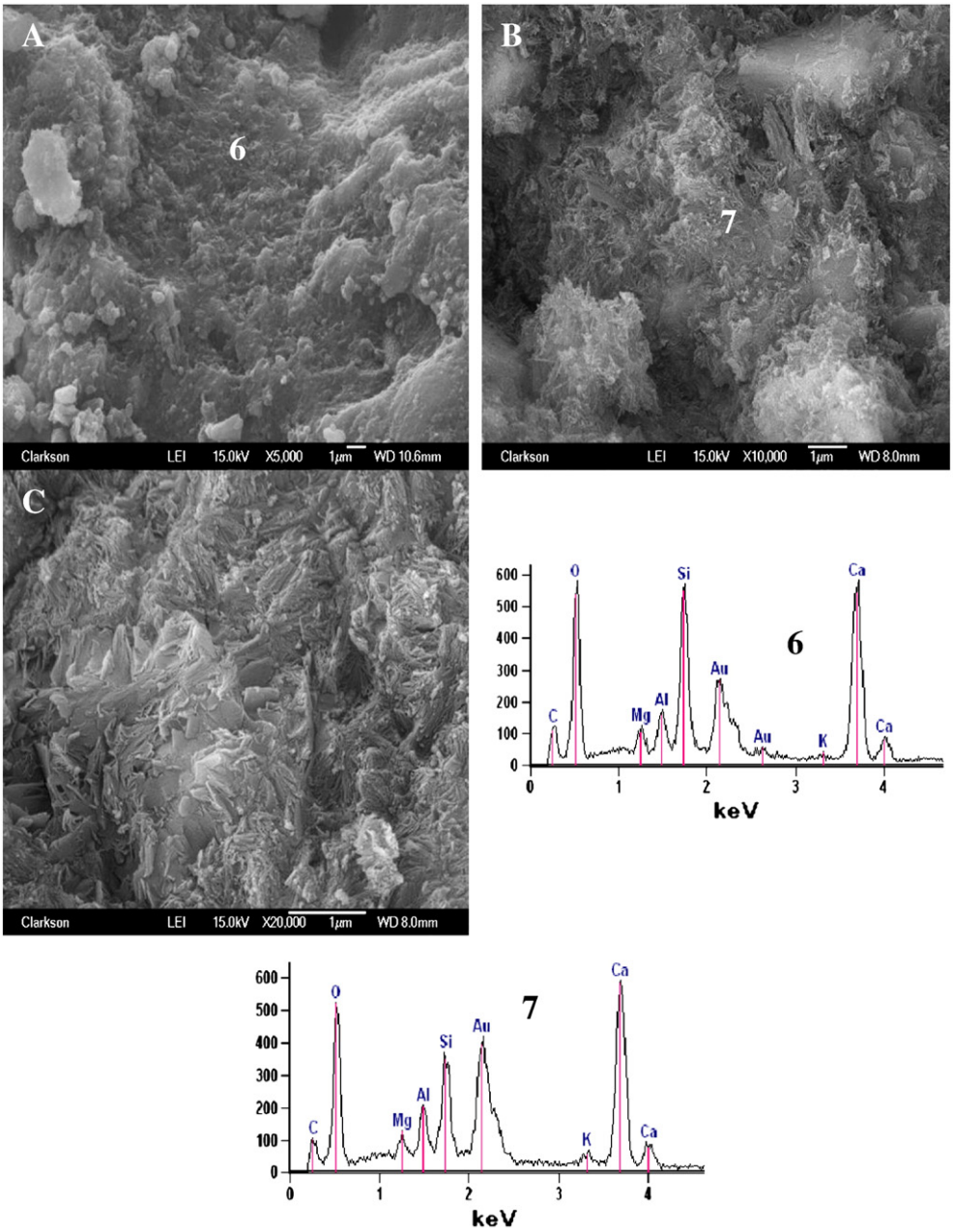

Fig. 10. SEM micrographs of heat cured CKD–GGBFS paste after 28 days of lime curing with EDXs at locations 6 and 7.

curing despite the substantial strength developed during this period. Hence, we can conclude that only a part of the initial strength developed in the CKD–GGBFS binder can be attributed to the ettringite. Any further strength improvement should be due to the formation of the C-S-H in the system.

Formation of a thin coating on the surface of the slag particle when it comes into contact with water has been suggested as the mechanism for latent hydraulic reactivity of slag [9]. In a recent study, the formation of a reaction shell was observed on the surface of the fly ash particles during the SEM examination of the CKD-fly ash paste [34]. However, in the present study, a similar type of topo-chemical reaction shell was not observed on the surface of the GGBFS particles. In the CKD–GGBFS system, most of the slag particles appeared to be completely dissolved. Only a few partially dissolved slag particles were identified during the SEM examination. Most of the locations that were examined in the CKD–GGBFS system resembled the microstructure shown in micrographs B, C and D presented in Fig. 11.

The hypothesis of the research was based on the premise that the alkalis and sulfates present in the CKD will accelerate the reactivity of GGBFS and form an alkali incorporated binding product. A small potassium peak was consistently present in all EDX spectra collected from the C-S-H gels indicating the incorporation of potassium in the reaction product structure supporting this hypothesis. This peak persisted in the samples subjected to longer periods of wet curing indicating that potassium was not leached out of the system due to soaking (see EDX analysis presented in Figs. 9 and 10). However, the role of alkalis in activating the GGBFS could not be determined unequivocally in the present study since only one CKD was used for the analysis. It is worth noting that there is a wide variation in the composition of CKDs [21,22]. As per the classification proposed in our previous studies [22–24], the present CKD can be classified as a low

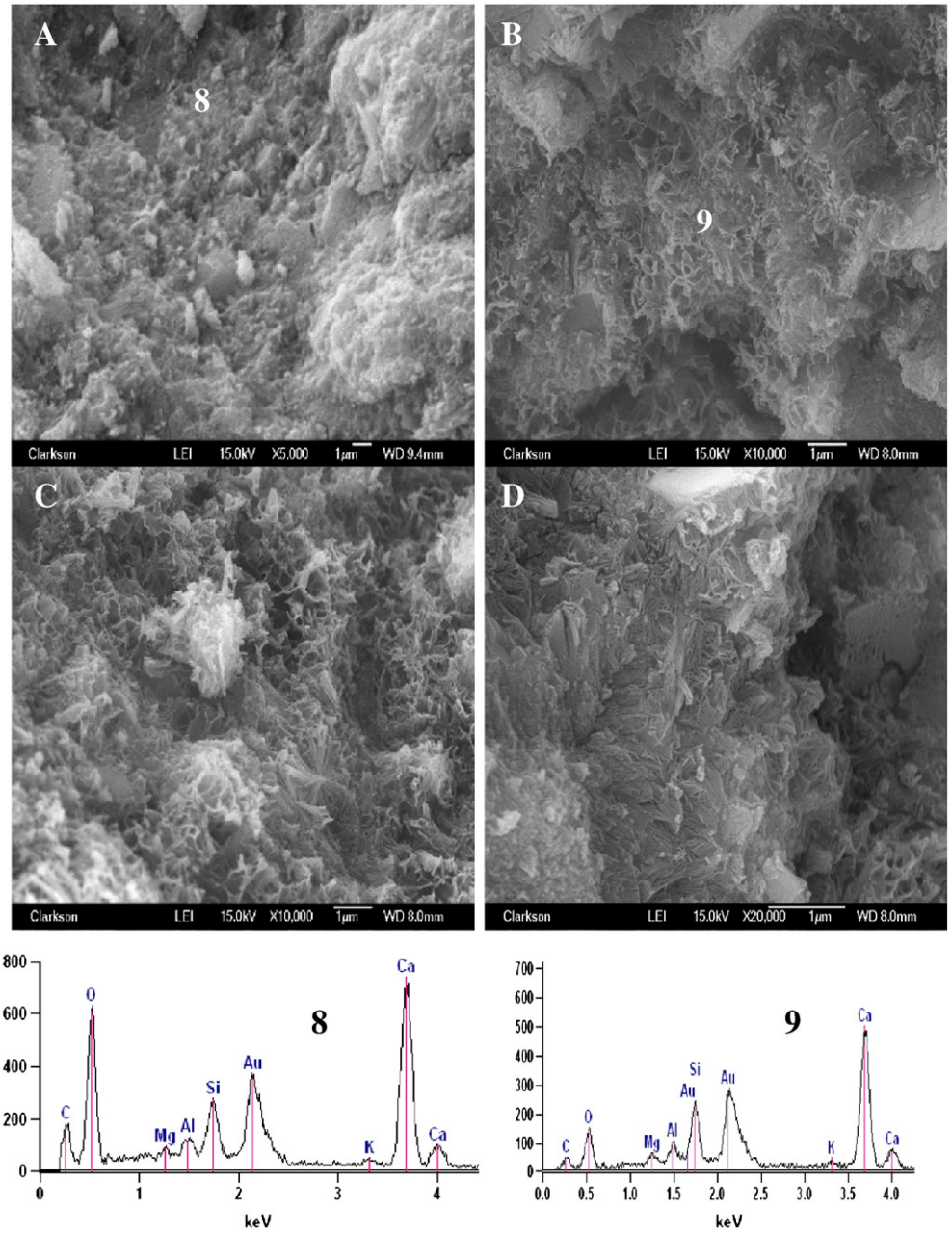

Fig. 11. SEM micrographs of moist cured CKD–GGBFS paste after 28 days with EDX patterns at locations 8 and 9.

free lime content CKD with ~4.5% free lime, 3.5% alkalis and 10% sulfate. In most of the existing beneficial utilization of CKDs, high free lime content CKDs are preferred since they perform well in these applications including soil stabilization compared to the low lime CKDs. Findings of the present study demonstrate the potential of low lime CKDs for its beneficial usage. Though the effectiveness of the particular CKD used in the present study in activating GGBFS should not be taken as representative for CKDs in general, the reaction mechanism in the CKD–GGBFS system and its dependence on the CKD's properties, as identified in this study, are both expected to be present at varying degrees in other CKD–GGBFS systems. Hence, the findings of the present study may offer general guidelines to estimate the effectiveness of the CKDs in activating GGBFS. As described before, a higher dosage of CKD (70%) was necessary to activate the slag, and this percentage may vary depending upon the chemical composition of a given CKD.

It is also important to note that the CKD–GGBFS binder at a water-to-binder ratio of 0.40 resulted in a 60% flow value (Fig. 4 (B)), which is very low from the field application point of view. However, in our later studies it was found that workability can be improved by the addition of high range water reducers. Lower workability of these mixtures should be improved for the successful application of this material in the field.

5. Conclusion

The CKD, with a low free lime and high sulfate and alkali content, used in this study was effective in accelerating the hydration of GGBFS. The CKD–GGBFS paste achieved a compressive strength up to 35 MPa. The strength development rate was found to be dependent on the curing conditions but eventually all the samples achieved similar compressive strengths independent of the curing conditions. Mineralogical and

microstructural examinations identified the formation of calcium silicate hydrate (C-S-H, C-A-S-H and C-A-M-S-H) and ettringite in CKD–GGBFS binder. Ettringite appeared to contribute significantly to the early stage of of strength development. However, results clearly show that the later age strength development is dominated by the extensive formation of C-S-H. Hence the findings of the present study might lead to the beneficial usage of low free lime content CKD in future.

Acknowledgements

The authors thank Mr. Paul Brook of Holcim Ltd. for providing the CKD material and the oxide analysis presented in Table 1. In addition, the second author personally would like to thank the late Jean-Claude Roumain (J.C.), former corporate producer manager Holcim Ltd. (USA) for constructive discussions.

References

[1] E. Douglas, J. Brandstetr, A preliminary study on the alkali activation of ground granulated blast-furnace slag, Cem. Concr. Res. 20 (5) (1990) 746–756.
[2] J. Davidovits, Geopolymers: inorganic polymeric new materials, J. Therm. Anal. 37 (8) (1991) 1633–1656.
[3] A. Palomo, M.W. Grutzeck, M.T. Blanco-Varela, Alkali activated fly ashes: a cement for the future, Cem. Concr. Res. 29 (8) (1999) 1323–1329.
[4] A. Fernández-Jiménez, J.G. Palomo, F. Puertas, Alkali-activated slag mortars: mechanical strength behavior, Cem. Concr. Res. 29 (8) (1999) 1313–1321.
[5] C. Shi, R.L. Day, Early strength development and hydration of alkali-activated blast furnace slag/fly ash blends, Adv. Cem. Res. 11 (4) (1999) 189–196.
[6] A. Fernández-Jiménez, A. Palomo, Composition and microstructure of alkali activated fly ash binder: effect of the activator, Cem. Concr. Res. 35 (10) (1984–1992) 1984–1992.
[7] A. Fernández-Jiménez, F. Puertas, Alkali-activated slag cements: kinetics studies, Cem. Concr. Res. 27 (3) (1997) 359–368.
[8] D.L.Y. Kong, J.G. Sanjayan, K. Sagoe-Crentsil, Comparative performance of geopolymers made with metakaolin and fly ash after exposure to elevated temperatures, Cem. Concr. Res. 37 (5) (2007) 1583–1589.
[9] M. Regourd, J.H. Thomassin, P. Baillif, J.C. Touray, Blast-furnace slag hydration: surface analysis, Cem. Concr. Res. 13 (4) (1983) 549–556.
[10] C. Shi, R.L. Day, Some factors affecting early hydration of alkali-slag cements, Cem. Concr. Res. 26 (3) (1996) 439–447.
[11] C. Shi, Y. Li, Investigation on some factors affecting the characteristics of alkali-phosphorus slag cement, Cem. Concr. Res. 19 (4) (1989) 527–533.
[12] S.D. Wang, K.L. Scrivener, P.L. Pratt, Factors affecting the strength of alkali activated slag, Cem. Concr. Res. 24 (6) (1994) 1033–1043.
[13] C. Shi, R.L. Day, A calorimetric study of early hydration of alkali-slag cements, Cem. Concr. Res. 25 (6) (1995) 1333–1346.
[14] T. Bakharev, J.G. Sanjayan, Y.B. Cheng, Effect of elevated temperature curing on properties of alkali-activated slag concrete, Cem. Concr. Res. 29 (10) (1999) 1619–1625.
[15] S.J. Barnett, M.N. Soutsos, S.G. Millard, J.H. Bungey, Strength development of mortars containing ground granulated blast-furnace slag: effect of curing temperature and determine of apparent activation energies, Cem. Concr. Res. 36 (3) (2006) 434–440.
[16] D. Ravikumar, S. Peethamparan, N. Neithalath, Structure and strength of NaOH activated concretes containing fly ash or GGBFS as the sole binder, Cem. Concr. Compos. 32 (6) (2010) 399–410.
[17] H.F.W. Taylor, Cement Chemistry, 2nd Edition, Thomas Telford, London, 1997.
[18] M.C.G. Juenger, P.J.M. Monteiro, E.M. Gartner, In-situ imaging of ground granulated blast furnace slag hydration, J. Mater. Sci. 41 (21) (2006) 7074–7081.
[19] A.M. Amin, E. Ebied, H. El-Didamony, Activation of granulated slag with calcined cement dust, Silic. Indus. 60 (3–4) (1995) 109–115.
[20] H. El-Didamony, A.H. Aly, A.M. Sharara, A.M. Amin, Assessment of cement dust with anhydrite as an activator for granulated slag, Silic. Indus. 62 (1–2) (1997) 31–36.
[21] M.S. Konsta-Gdoutos, S.P. Shah, Hydration and properties of novel blended cements based on cement kiln dust and blast furnace slag, Cem. Concr. Res. 33 (8) (2003) 1269–1276.
[22] S. Peethamparan, J. Olek, J. Lovell, Influence of chemical and physical characteristic of cement kiln dusts (CKDs) on their hydration behavior and potential application in soil stabilization, Cem. Concr. Res. 38 (2008) 803–815.
[23] S. Peethamparan, J. Olek, S. Diamond, Mechanism of stabilization of Na-montmorillonite clay with cement kiln dust, Cem. Concr. Res. 36 (7) (2009) 580–589.
[24] S. Peethamparan, J. Olek, A study on the effectiveness of cement kiln dusts (CKDs) in stabilizing Na-montmorillonite clay, J. Mater. Civ. Eng. 20 (2) (2008) 137–146.
[25] ASTM C 1437, Standard Test Method for Flow of Hydraulic Cement Mortar, ASTM International, West Conshohocken, PA, 2001.
[26] ASTM C 191, Standard Test Method for Time of Setting of Hydraulic Cement by Vicat Needle, ASTM International, West Conshohocken, PA, 2001.
[27] N.C. Collier, J.H. Sharp, N.B. Milestone, J. Hill, I.H. Godfrey, The influence of water removal techniques on the composition and microstructure of hardened cement pastes, Cem. Concr. Res. 38 (6) (2008) 737–744.
[28] L. Alarcon-Ruiz, G. Platret, E. Massieu, A. Ehrlacher, The use of thermal analysis in assessing the effect of temperature on a cement paste, Cem. Concr. Res. 35 (3) (2005) 609–613.
[29] C. Alonso, L. Fernandez, Dehydration and rehydration processes of cement paste exposed to high temperature environments, J. Mater. Sci. 39 (9) (2004) 3015–3024.
[30] J.B. Odelson, E.A. Kerr, W. Vichit-Vadakan, Young's modulus of cement paste at elevated temperatures, Cem. Concr. Res. 37 (2) (2007) 258–263.
[31] I.G. Richardson, G.W. Groves, Microstructure and microanalysis of hardened cement pastes involving ground granulated blast-furnace slag, J. Mater. Sci. 27 (22) (1992) 6204–6212.
[32] I.G. Richardson, A.R. Brough, G.W. Groves, C.M. Dobson, The characterization of hardened alkali-activated blast furnace slag pastes and the nature of the calcium silicate hydrate (C-S-H) phase, Cem. Concr. Res. 24 (5) (1994) 813–829.
[33] S.D. Wang, K.L. Scrivener, Hydration products of alkali activated slag cement, Cem. Concr. Res. 25 (3) (1995) 561–571.
[34] P. Chaunsali, S. Peethamparan, Microstructural and mineralogical characterization of cement kiln dust-activated fly ash binder, Transp. Res. Rec. 2164 (2010) 36–45.